Nanogap plasmonic field enhancement on hydrogen-absorbing transition metals

AUTHOR NAMES

Yuki Nakashima and Katsuaki Tanabe*

AUTHOR ADDRESS

Department of Chemical Engineering, Kyoto University, Nishikyo, Kyoto 615–8510, Japan

AUTHOR INFORMATION

Corresponding Author

*Email: tanabe@cheme.kyoto-u.ac.jp

KEYWORDS

transition metal; surface plasmon; gap plasmon; nanoparticle; nanophotonics; hydrogen storage; sensing; nuclear fusion; energy device

ABSTRACT

The electromagnetic field enhancement factors by gap plasmons between two spherical metal particles are calculated for hydrogen-absorbing transition metals Pd, Ti, and Ni, and reference noble metals Au, Ag, and Cu, in air, H_2, or vacuum, and H_2O. The dependence of the field enhancement factors on the metal species, the field wavelength, the electric field polarization, the separation of the two metal particles, and the observing location is systematically investigated. Field enhancement is observed significantly large in the gap of two metal particles and sensitive to the particle separation, but insensitive to the position in the gap, indicating a geometric flexibility for applications. The spectral peak field enhancement factors for Pd, Ti, and Ni do not compete with those for Au, Ag, and Cu, but do in the microwave regime. For the electric field parallel to the bipartite alignment, the field enhancement factors in the gap for Pd, Ti, and Ni are observed as large as several hundred and ten thousand for the separation-to-radius ratios of 0.1 and 0.01, respectively, for a wide wavelength region spanning from the visible to the infrared. The large field enhancements in the nanogaps of hydrogen-absorbing transition metals observed in this study can potentially be utilized for various energy applications, such as hydrogen storage, sensing, and nuclear fusion. In practical metallic material systems, it is important to account for such a gap-plasmon effect because nanoscale gaps commonly exist, for instance, on rough metal surfaces and in metal particle aggregates.

I. INTRODUCTION

Hydrogen-absorbing metals are thought to be an important technological component for energy applications today.[1–6] Free electrons in metallic materials, particularly around metal surfaces or interfaces with dielectric materials, exhibit a strong interaction with electromagnetic fields or light in the form of collective oscillation, named *surface plasmons*.[7–12] Surface-plasmon-induced electromagnetic field enhancement on noble metal surfaces has been utilized for various applications, such as chemical and biomedical sensing, light emitters and detectors, and optical cloaking.[7–12] The plasmonic field enhancement effect on hydrogen-absorbing transition metals also has a number of potential applications, such as hydrogen storage,[1–6] sensing,[13–16] and nuclear fusion.[17–21] Noble metals such as Au, Ag, and Cu are known to exhibit large plasmonic field enhancements particularly at optical frequencies and have been considerably investigated in the context of plasmonics, both experimentally and theoretically.[7–12] In contrast, the surface-plasmon behavior for hydrogen-absorbing transition metals has not been well studied yet. Experimentally, Langhammer *et al.* introduced a plasmonic hydrogen sensing scheme by detecting the induced electronic and structural changes in Pd during the hydridation process.[13,16] Liu *et al.* demonstrated plasmonic Au nanoantenna-enhanced hydrogen sensing via hydrogen absorption in Pd.[14] Baldi *et al.* realized *in-situ* detection of hydrogen-induced phase transitions in individual Pd nanocrystals by electron energy-loss spectroscopy.[15] Nevertheless, quantitative and systematic analysis of the field enhancement effect for hydrogen-absorbing metals on conditions, which is required for the design and optimization of practical systems, had not been reported. Because of such a motivation, we previously calculated the plasmonic field enhancement factors on planar[22] and spherical[23,24] surfaces and also at sharp tips[24] of

nanoparticles or nanoscale surface roughnesses of hydrogen-absorbing transition metals. We therein showed that a large degree of energy focusing, with the enhancement factor over several hundred, is available on the planar surface of Pd, Ti, and Ni in the microwave region, even surpassing the enhancement for noble metals. We also calculated large field enhancements at sharp tips of nanoparticles or nanoscale surface roughnesses of these hydrogen-absorbing transition metals, such as peak field enhancement factors of 6000 and 2×10^8 in air for morphological aspect ratios of 10 and 100, respectively, for Pd. It is also known that surface plasmons in between multiple metallic objects with nanoscale separation distances, or so-called *gap plasmons*, provide large field enhancement factors.[25–30] Consideration of the gap-plasmon effect for hydrogen-energy applications is important because nanogaps commonly exist in real structures such as rough metal surfaces and ensembles of metal particles. Therefore, in the present study, we numerically investigate the plasmonic field enhancement in nanogaps of hydrogen-absorbing transition metals, Pd, Ti, and Ni.

II. THEORY AND CALCULATION METHODS

Based on the method presented by Aravind *et al.*,[25] we calculate the electromagnetic field enhancement factors in nanogaps between two spherical metal nanoparticles. The field enhancement factor is defined as the ratio of the electromagnetic field intensity around the object, which is a pair of metal particles in this study, to that in the absence of the object, or the original incident field. Figure 1 conceptually depicts the model setup. The z-axis passes both of the centers of the two metal particles, and the x–y plane at $z = 0$ is the symmetric mirror plane of the particles. For the cases where the particle sizes are smaller than the wavelength of the

electromagnetic field, the quasistatic approximation is applicable, and therefore the field enhancement factors can be determined by solving the Laplace equations derived from the Maxwell equations. In addition, the solutions can be relatively easily obtained by using the bispherical coordinate system (μ, η, ϕ)[31] for the bipartite system. The bispherical coordinate system is a three-dimensional rectangular coordinate system formed by rotating the two-dimensional bipolar coordinate system with a rotation axis passing the two focal points. The relationship between the bispherical (μ, η, ϕ) and rectangular (x, y, z) coordinate systems is expressed as follows:

$$x = \frac{a \sin\eta \cos\phi}{\cosh\mu - \cos\eta}, \quad (1)$$

$$y = \frac{a \sin\eta \sin\phi}{\cosh\mu - \cos\eta}, \quad (2)$$

$$z = \frac{a \sinh\mu}{\cosh\mu - \cos\eta}, \quad (3)$$

$$\mu = \operatorname{arcsinh}\left(\frac{2az}{\sqrt{\left(x^2 + y^2 + z^2 + a^2\right)^2 - \left(2az\right)^2}} \right), \quad (4)$$

$$\eta = \arccos\left(\frac{x^2 + y^2 + z^2 - a^2}{\sqrt{\left(x^2 + y^2 + z^2 + a^2\right)^2 - \left(2az\right)^2}} \right), \quad (5)$$

$$\phi = \arctan\left(\frac{y}{x}\right). \quad (6)$$

a is the z-axis value of the focal point, and can be determined by:

$$a = R_0\sqrt{\left(1+\frac{D}{2R_0}\right)^2 - 1}\,, \quad (7)$$

where R_0 and D are the radius and separation of the particles, respectively. $\mu = 0$ corresponds to the x–y mirror plane at $z = 0$, and $\mu = \mu_0$ and $-\mu_0$ correspond to the surface of the upper and lower particles, respectively, in the bipartite model. μ_0 is determined by:

$$\mu_0 = \operatorname{arccosh}\left(1+\frac{D}{2R_0}\right). \quad (8)$$

The boundary conditions for the electrostatic potentials of in the surrounding medium, the lower particle with the surface $\mu = -\mu_0$, and the upper particle with the surface $\mu = \mu_0$, Φ_0, Φ_1, and Φ_2, respectively, are expressed as follows:

$$\Phi_0\big|_{\mu=-\mu_0} = \Phi_1\big|_{\mu=-\mu_0}\ , \quad (9)$$

$$\Phi_0\big|_{\mu=\mu_0} = \Phi_2\big|_{\mu=\mu_0}\ , \quad (10)$$

$$\epsilon_0 \frac{\partial \Phi_0}{\partial \mu}\big|_{\mu=-\mu_0} = \epsilon(\lambda) \frac{\partial \Phi_1}{\partial \mu}\big|_{\mu=-\mu_0}, \quad (11)$$

$$\epsilon_0 \frac{\partial \Phi_0}{\partial \mu}\big|_{\mu=\mu_0} = \epsilon(\lambda) \frac{\partial \Phi_2}{\partial \mu}\big|_{\mu=\mu_0}, \quad (12)$$

where ε_0 and $\varepsilon(\lambda)$ are the complex permittivities or dielectric functions of the surrounding medium and the metal, respectively, and λ is the freespace wavelength. From these boundary conditions and the Laplace equations, Φ_0, Φ_1, and Φ_2 are expressed as follows:

$$\Phi_0 = \Phi^{\text{ext}} + F \sum_{n\geq|m|}^{\infty} \sum_{m=-\infty}^{\infty} \left\{ A_n^m \exp\left[\left(n+\frac{1}{2}\right)\mu\right] + B_{\text{n}}^{\text{m}} \exp\left[-\left(n+\frac{1}{2}\right)\mu\right]\right\} Y_n^m(\cos\eta,\phi)$$

$$\left(-\mu_0 < \mu < \mu_0\right), \quad (13)$$

$$\Phi_1 = F \sum_{n\geq|m|}^{\infty} \sum_{m=-\infty}^{\infty} D_n^m \exp\left[\left(n+\frac{1}{2}\right)\mu\right] Y_n^m(\cos\eta,\phi) \quad \left(\mu < -\mu_0\right), \quad (14)$$

$$\Phi_2 = F \sum_{n\geq|m|}^{\infty} \sum_{m=-\infty}^{\infty} C_n^m \exp\left[-\left(n+\frac{1}{2}\right)\mu\right] Y_n^m(\cos\eta,\phi) \quad \left(\mu > \mu_0\right), \quad (15)$$

$$F \equiv \sqrt{\cosh\mu - \cos\eta}\,. \quad (16)$$

Φ^{ext} is the potential for the external electric field, $Y_n^m(\cos\eta,\ \phi)$ is the spherical harmonics, and A_n^m, B_n^m, C_n^m, and D_n^m are constants to be determined by the boundary conditions. Φ^{ext} is expressed by:

$$\Phi^{\text{ext}} = -E_0\left(z\cos\theta_0 + x\sin\theta_0\cos\phi_0 + y\sin\theta_0\sin\phi_0\right), \quad (17)$$

where E_0 is the amplitude of the external electric field, and θ_0 and ϕ_0 are the polar and azimuthal angles of the direction of the external electric field relative to the *z*- and *x*-axes, respectively, as indicated in Fig. 1. The spherical harmonics are expressed by:[32]

$$Y_n^m\left(\cos\eta,\phi\right) = \left(-1\right)^{\frac{m+|m|}{2}}\sqrt{\frac{2n+1}{4\pi}\frac{\left(n-|m|\right)!}{\left(n+|m|\right)!}}\,P_n^{|m|}\left(\cos\eta\right)\mathrm{e}^{\mathrm{i}m\phi}, \quad (18)$$

$$P_n^m\left(t\right) = \frac{1}{2^{\mathrm{n}}}\left(1-t^2\right)^{\frac{m}{2}}\sum_{j=0}^{\left\lfloor\frac{n-m}{2}\right\rfloor}\frac{\left(-1\right)^j\left(2n-2j\right)!}{j!\left(n-j\right)!\left(n-2j-m\right)!}t^{n-2j-m}\,. \quad (19)$$

A_n^m, B_n^m, C_n^m, and D_n^m can be determined, via Eqs. 9–12, through the following equations. For *m*

$= 0,$

$$A_n^0 = -B_n^0, \quad (20)$$

$$C_n^0 = -D_n^0, \quad (21)$$

$$C_n^0 = \{\exp\left[\left(2n+1\right)\mu_0\right]-1\}A_n^0 - F_0\cos\theta_0\sqrt{4\pi\left(2n+1\right)}, \quad (22)$$

$$U_n^0 A_n^0 + V_n^0 A_{n-1}^0 + W_n^0 A_{n+1}^0 = S_n^0, \quad (23)$$

$$U_n^0 = \chi\sinh\mu_0\left\{1-\exp\left[-\left(2n+1\right)\mu_0\right]\right\} + \left(2n+1\right)\cosh\mu_0\left\{1+\chi\exp\left[-\left(2n+1\right)\mu_0\right]\right\}, \quad (24)$$

$$V_n^0 = -n\sqrt{\frac{2n-1}{2n+1}}\exp\left(-\mu_0\right)\left\{1+\chi\exp\left[-\left(2n-1\right)\mu_0\right]\right\}, \quad (25)$$

$$W_n^0 = -\left(n+1\right)\sqrt{\frac{2n+3}{2n+1}}\exp\left(\mu_0\right)\left\{1+\chi\exp\left[-\left(2n+3\right)\mu_0\right]\right\}, \quad (26)$$

$$S_n^0 = 2F_0\cos\theta_0\,\chi\exp\left[-\left(2n+1\right)\mu_0\right]\sqrt{\frac{4\pi}{2n+1}}\left\{\cosh\mu_0 - \left(2n+1\right)\sinh\mu_0\right\}, \quad (27)$$

$$F_0 \equiv aE_0\sqrt{2}, \quad (28)$$

$$\chi \equiv \frac{\left[\epsilon_0 - \epsilon\left(\lambda\right)\right]}{\left[\epsilon_0 + \epsilon\left(\lambda\right)\right]}. \quad (29)$$

For $m = 1$ and -1,

$$A_n^{\pm 1} = B_n^{\pm 1}, \quad (30)$$

$$A_n^{-1} = -\exp\left(2\mathrm{i}\phi_0\right) A_n^1, \quad (31)$$

$$C_n^{\pm 1} = D_n^{\pm 1}, \quad (32)$$

$$C_n^{-1} = -\exp\left(2\mathrm{i}\phi_0\right) C_n^1, \quad (33)$$

$$C_n^1 = \{\exp\left[\left(2n+1\right)\mu_0\right]+1\} A_n^1 + F_0 \sin\theta_0 \exp\left(-i\phi_0\right)\sqrt{\frac{4\pi n\left(n+1\right)}{2n+1}}, \quad (34)$$

$$U_n^1 A_n^1 + V_n^1 A_{n-1}^1 + W_n^1 A_{n+1}^1 = S_n^1, \quad (35)$$

$$U_n^1 = \chi \sinh\mu_0 \left\{1+\exp\left[-\left(2n+1\right)\mu_0\right]\right\} + \left(2n+1\right)\cosh\mu_0 \left\{1-\chi\exp\left[-\left(2n+1\right)\mu_0\right]\right\}, \quad (36)$$

$$V_n^1 = -\sqrt{\frac{\left(n+1\right)\left(n-1\right)\left(2n-1\right)}{2n+1}}\ \exp\left(-\mu_0\right)\left\{1-\chi\exp\left[-\left(2n-1\right)\mu_0\right]\right\}, \quad (37)$$

$$W_n^1 = -\sqrt{\frac{n\left(n+2\right)\left(2n+3\right)}{2n+1}}\ \exp\left(\mu_0\right)\left\{1-\chi\exp\left[-\left(2n+3\right)\mu_0\right]\right\}, \quad (38)$$

$$S_n^1 = 2F_0 \sin\theta_0 \sinh\mu_0 \chi \exp\left(-\mathrm{i}\phi_0\right)\exp\left[-\left(2n+1\right)\mu_0\right]\sqrt{\frac{4\pi n\left(n+1\right)}{2n+1}}. \quad (39)$$

For other integer values of m, ${A_n}^m$, ${B_n}^m$, ${C_n}^m$, and ${D_n}^m$ are zero. ${A_n}^m$, ${B_n}^m$, ${C_n}^m$, and ${D_n}^m$ also become zero for m = 1 and –1 when the external electric field is parallel to the z-axis ($\theta_0 = 0$), and for m = 0 when the external electric field is perpendicular to the z-axis ($\theta_0 = \pi/2$). For n = 0 and $n_{\max}$, the maximum value of n, Eq. 23 becomes:

$$U_0^0 A_0^0 + W_0^0 A_1^0 = S_0^0, \quad (40)$$

$$U_{n_{\max}}^0 A_{n_{\max}}^0 + V_{n_{\max}}^0 A_{n_{\max}-1}^0 = S_{n_{\max}}^0 . \quad (41)$$

For n = 1 and $n_{\max}$, Eq. 35 becomes:

$$U_1^1 A_1^1 + W_1^1 A_2^1 = S_1^1, \quad (42)$$

$$U_{n_{\max}}^1 A_{n_{\max}}^1 + V_{n_{\max}}^1 A_{n_{\max}-1}^1 = S_{n_{\max}}^1 . \quad (43)$$

For each condition of the system, we need to solve the simultaneous equations of Eqs. 23 and 35 with a sufficiently large $n_{\max}$, for the convergence of ${A_n}^m$, ${B_n}^m$, ${C_n}^m$, ${D_n}^m$, and the below-mentioned field enhancement factor. Their convergence becomes laborious as the two particles become closer to each other, and $n_{\max}$ of about 100 was required for the case D/R_0 = 0.01, for example. ${A_n}^m$, ${B_n}^m$, ${C_n}^m$, and ${D_n}^m$ determined by Eqs. 20–39 satisfy Eqs. 9–12.

After determining A_n^m, B_n^m, C_n^m, and D_n^m, we calculate the electric field components E_μ, E_η, and E_ϕ with the scaling factors h_μ, h_η, and h_ϕ as follows:

$$E_i = \frac{1}{h_i}\frac{\partial \Phi_0}{\partial i} \quad (i = \mu,\ \eta,\ \phi), \quad (44)$$

$$h_\mu = \frac{a}{\cosh\mu - \cos\eta}, \quad (45)$$

$$h_\eta = \frac{a}{\cosh\mu - \cos\eta}, \quad (46)$$

$$h_\phi = \frac{a\sin\eta}{\cosh\mu - \cos\eta}. \quad (47)$$

Finally, we calculate the electromagnetic field enhancement factor I by:

$$I = \frac{E_\mu E_\mu^* + E_\eta E_\eta^* + E_\phi E_\phi^*}{E_0 E_0^*}, \quad (48)$$

where the superscript * denotes the complex conjugate of each field component.

For the calculations, we used *Python 3* with the libraries *NumPy* and *SciPy*. We employed the

method *numpy.linalg.solve* to solve the simultaneous equations. For the derivative calculations, we used the central difference scheme with a step width of 10^{-4}. We employed the empirical complex dielectric functions of metals and of the surroundings on frequencies listed in Refs. 22, 23, and 33 for the calculations in this study. We calculated the electromagnetic field enhancement factors at the points on the x–z plane at $y = 0$, i.e., $\phi = 0$, with the external electric field parallel to the plane, i.e., $\phi_0 = 0$. For the convergent calculations, we set $n_{max} = 150$. For the calculations for the points of $\theta = 0, \pi$, where θ is the polar angle of the observing point relative to the z-axis as indicated in Fig. 1, we calculated with $x/R_0 = 10^{-4}$ instead of $x = 0$ to circumvent diverging numerical errors.

III. RESULTS AND DISCUSSION

We firstly present a series of calculation results of the electromagnetic field enhancement for the case of the surrounding medium of air, H_2, or vacuum. Figure 2 (a) presents the spectra of field enhancement factor for Pd particles in air, H_2, or vacuum, for the condition $\theta_0 = 0$, $\theta = \pi$, and $D/R_0 = 0.1$, with various d/D. d is the distance between the observing point and the surface of the particle, as indicated in Fig. 1. The condition $\theta_0 = 0$ corresponds that the external electric field is parallel to the line between the centers of the two metal particles. The condition $\theta = \pi$ corresponds that the observing point is on the line between the centers of the two metal particles. The ratio D/R_0 is the separation of the particles normalized by the radius of the particles, as schematically depicted in Fig. 1. The ratio d/D is the distance between the observing point and the surface of the particle normalized by the separation of the particles. Field enhancement factors of several hundred are observed in the results of Fig. 2 (a). These field enhancements are

significantly larger than those for an isolated, single spherical Pd particle reported in Ref. 23, and thus exhibiting the effect of gap plasmons. This Pd-particle system exhibits a plasmon resonance at 365 nm. Interestingly, the variation in the position of the observing point between the particles, d/D, has a relatively small influence on the field enhancement, indicating a preferable spatial flexibility for applications. To analyze the dependence of the polarization of the electric field on the field enhancement, Figures 2 (b) and (c) plot the calculated spectra of electromagnetic field enhancement factor for Pd particles in air, H_2, or vacuum, for the condition θ_0 = (b) $\pi/2$, (c) $\pi/4$, $\theta = \pi$, and $D/R_0 = 0.1$, with various d/D, with the only difference from Fig. 2 (a) being the values of θ_0. The quantitative result for the case of $\theta_0 = \pi/4$ in Fig. 2 (c) is observed to be the average of those for $\theta_0 = 0$ in Fig. 2 (a) and $\theta_0 = \pi/2$ in Fig. 2 (b), for the principle of superposition. As observed among Figs. 2 (a)–(c), for other polarization angles than $\theta_0 = 0$, the field enhancement becomes weaker, as commonly known for the single-particle case.[23] Therefore, we mainly focus on the case $\theta_0 = 0$, corresponding to the external electric field parallel to the line between the centers of the two metal particles, in this study.

Figure 3 presents the calculated electromagnetic field enhancement factors for Pd particles in air, H_2, or vacuum, for the condition $\theta_0 = 0$, $d/D = 0$, and $\lambda = 365$ nm, which is the resonant wavelength observed in Fig. 2 (a), with various θ and D/R_0. In other words, this calculation rotationally tracks the field enhancement on the surface of the particle ($d/D = 0$) for the angular dependence of the observing point (θ). The calculation result of the field enhancement factors for the condition $D/R_0 = 100$ approximately corresponds to those for the monopartite case,[23] with a periodic angular evolution equivalently peaking at $\theta = 0$ and π. For $D/R_0 = 0.1$, which is the same setting as Fig. 2 and the regime of gap plasmon, it is observed that the field enhancement factor

has a sharp peak at $\theta = \pi$, whose value is significantly larger than that at $\theta = 0$, in contrast to the case of $D/R_0 = 100$. Reflecting this result, hereafter we focus on the case $\theta = \pi$, corresponding to the observing point locating on the line between the centers of the two metal particles, in this study.

Figure 4 presents the calculated spectra of electromagnetic field enhancement factor for Pd particles in air, H_2, or vacuum, for the condition $\theta_0 = 0$, $\theta = \pi$, and d/D = (a) 0, (b) 0.5, with various D/R_0. The result for $D/R_0 = 100$, which asymptotically corresponds to the isolated-particle case, in Fig. 4 (a) is consistent with those presented in the previous numerical studies for single Pd particles.[23,24] Field enhancement factors over ten thousand are observed for the case $D/R_0 = 0.01$. It is also observed in Figs. 4 (a) and (b) that the field enhancement factor is sensitive to the scale of D/R_0, or the separation of the two metal particles, and is about a thousand for $D/R_0 = 0.05$. The setting $d/D = 0.5$ of Fig. 4 (b) corresponds to the situation that the observing point locates exactly at the midst of the two metal particles, while $d/D = 0$ for Fig. 4 (a) positions at the surface of a particle. Comparing between Figs. 4 (a) and (b), the insensitivity of field enhancement on the position between the particles is observed and thus being preferable for applications, as discussed for the result of Fig. 2 (a).

In addition to the presentation of Figs. 2–4, for the potential convenience for the readers, a comprehensive set of the calculation results for Pd, Ti, Ni, Au, Ag, and Cu under various series of conditions is provided in Supplementary Material. In our series of analogical calculations for other metals, Ti, Ni, Au, Ag, and Cu, the characteristic trends for Pd in Figs. 2–4 were similarly observed in Figs. S7–S66. As a cross-check for the correctness of our numerical calculations, the results in Figs. S51–S54 were consistent with the results for Ag presented in Ref. 25.

Here, we summarize the calculation results for hydrogen-absorbing transition metals Pd, Ti, and Ni and noble metals Au, Ag, and Cu traditionally studied in the field of plasmonics. Figure 5 presents the calculated spectra of electromagnetic field enhancement factor for various metal particles in air, H_2, or vacuum, for the condition $\theta_0 = 0$, $\theta = \pi$, $D/R_0 = 0.1$, 0.01, and $d/D = 0$, 0.5. For all kinds of metals, for each of the conditions $D/R_0 = 0.1$ and 0.01, the field enhancement factor does not largely vary with the value of d/D, 0 or 0.5, again indicating the spatial insensitivity in the gap. Particularly, there observed little visible difference between the plots of $d/D = 0$ (Fig. 5 (c)) and 0.5 (Fig. 5 (d)) for the case $D/R_0 = 0.01$. Such a similarity is presumably because even the location in the middle of the two metal particles is strongly influenced by both metal surfaces for the case of very narrow inter-particle gaps. For each condition of D/R_0 and d/D, the peak field enhancement factors in the spectra for Pd, Ti, and Ni do not compete with those for Au, Ag, and Cu. However, for the longer-wavelength or lower-frequency region, the field enhancement factors of all the metals converge and are comparable to one another. For the entire wavelength region, the field enhancement factors for Pd, Ti, and Ni exhibit values as large as several hundred and ten thousand for the cases $D/R_0 = 0.1$ and 0.01, respectively. These field enhancement factors observed are significantly larger than those for the single-particle case,[23] owing to the effect of gap plasmons. Interestingly, Ti is observed to be somewhat advantageous relative to other metals in the microwave regime.

Next, we present our calculation results for the case of the surrounding medium of H_2O, which is important for the applications in biomedical or electrolytic systems. Figure 6 presents the calculated spectra of electromagnetic field enhancement factor for various metal particles in H_2O, for the condition $\theta_0 = 0$, $\theta = \pi$, $D/R_0 = 0.1$, 0.01, and $d/D = 0$, 0.5. Similar to the case in in air, H_2, or vacuum, the field enhancement factors for each metal are not sensitive to the

observing position in the gap, d/D = 0 or 0.5. Particularly for the condition D/R_0 = 0.01, the plots for d/D = 0 (Fig. 6 (c)) and 0.5 (Fig. 6 (d)) are observed to be almost identical to each other. For the condition D/R_0 = 0.1, Pd, Ti, and Ni exhibit field enhancement factors of a couple of hundred throughout the wavelengths. Field enhancement factors over ten thousand are observed for Pd, Ti, and Ni for the wavelengths longer than the visible regime. Particularly, Ti exhibits peak field enhancement factors as large as thirty–forty thousand in the microwave region. The overall results of the field enhancement factor presented in Fig. 6 in H_2O are observed to be somewhat larger relative to those of Fig. 5 in air, H_2, or vacuum for each corresponding condition, except for the very short wavelength region below 400 nm. Such a trend of the superiority of H_2O as the surrounding medium is similar to those observed in the previous studies for the single-particle metallic systems.[23,24] This result of the large field enhancement factors in an aqueous medium is encouraging for electrolytic and biomedical applications.

Such large field enhancements in the nanogaps between particles of hydrogen-absorbing transition metals observed in this study can potentially be used for various hydrogen-related energy applications, as discussed in Refs. 22 and 24 in depth. It is important to account for the gap-plasmon effect in real material systems because nanoscale gaps are commonly observed, for instance, on rough metal surfaces and in metal-particle aggregates. The plasmonic field enhancement effect can be utilized, for example, for the enhancement of hydrogen absorption rate in hydrogen storage. Because the dissociative adsorption of gaseous hydrogen molecules is rate-determining for many metals and alloys, an active dissociation of hydrogen molecules into atoms or plasma by an applied electric field can potentially increase the hydrogen absorption rate.[22] In addition, it is indicated that hydrogen plasma enables supersaturation loading of hydrogen in metals.[34,35] The gap-plasmonic field enhancement can also be used for the

improvement of the optical sensitivity of hydrogen detection.[13–16] The field enhancement effect could be potentially also applicable to nuclear fusion,[17–21] as a scheme to increase the nuclear reaction rate by focusing the supplied electromagnetic field or laser on the fuel material containing hydrogen isotopes. As a final remark, a combination of the gap plasmon effect presented in this study with the nanoshell effect[23,36] and/or the lightning-rod effect[24,37] would provide further field enhancement.

IV. CONCLUSIONS

In this study, we calculated the electromagnetic field enhancement factors by gap plasmons between two spherical particles of hydrogen-absorbing transition metals Pd, Ti, and Ni, and reference noble metals Au, Ag, and Cu, in the media of air, H_2, or vacuum, and H_2O. We systematically analyzed the dependence of the field enhancement factors on the metal species, the field wavelength (λ), the electric field polarization (θ_0), the separation of the two metal particles (D/R_0), and the observing location (θ, d/D). Field enhancement was observed significantly large in the gap of two metal particles ($\theta = \pi$) and sensitive to D/R_0, but insensitive to d/D in the gap, indicating a preferable spatial flexibility for applications. The spectral peak field enhancement factors for Pd, Ti, and Ni do not compete with those for Au, Ag, and Cu, but do in the microwave regime. For the electric field parallel to the bipartite alignment ($\theta_0 = 0$), the field enhancement factors in the gap for Pd, Ti, and Ni were observed as large as several hundred and ten thousand for $D/R_0 = 0.1$ and 0.01, respectively, for a wide wavelength region through the visible to the infrared, for both of the surrounding media of in air, H_2, or vacuum, and H_2O. Such large field enhancements in the nanogaps between particles of hydrogen-absorbing transition

metals observed in this study could be used for various energy applications, such as hydrogen storage, sensing, and nuclear fusion. It is practically important to account for the gap-plasmon effect because nanoscale gaps commonly exist in real material systems, for example, on rough metal surfaces and in metal-particle aggregates. The field enhancement factors were found somewhat larger in H_2O than in air, H_2, or vacuum in the most wavelength regions, which is encouraging for the applications in biomedical or electrolytic systems. The gap-plasmonic field enhancement presented in this study could become even larger by combining with the nanoshell and lightning-rod effects.

SUPPLEMENTARY MATERIAL

See the supplementary material for Figs. S1–S66.

ACKNOWLEDGMENTS

The authors would like to thank Norihiko Fukuoka and Kosuke Nishigaya of Kyoto University for discussions. This study was supported, in part, by the Japan Society for the Promotion of Science (JSPS) and the Research Foundation for Opto-Science and Technology.

REFERENCES

[1] R. M. Stroud, A. M. Viano, P. C. Gibbons, K. F. Kelton, and S. T. Misture, "Stable Ti-based quasicrystal offers prospect for improved hydrogen storage," Appl. Phys. Lett. **69**, 2998–3000 (1996), https://doi.org/10.1063/1.117756.

[2] L. Schlapbach and A. Zuttel, "Hydrogen-storage materials for mobile applications," Nature **414**, 353–358 (2001), https://doi.org/10.1038/35104634.

[3] P. Tripodi, N. Armanet, V. Asarisi, A. Avveduto, A. Marmigi, J. D. Vinko, and J. P. Biberian, "The effect of hydrogenation/dehydrogenation cycles on palladium physical properties," Phys. Lett. A **373**, 3101–3108 (2009), https://doi.org/10.1016/j.physleta.2009.06.057.

[4] M. B. Ley, L. H. Jepsen, Y. S. Lee, Y. W. Cho, J. M. B. von Colbe, M. Dornheim, M. Rokni, J. O. Jensen, M. Sloth, Y. Filinchuk, J. E. Jorgensen, F. Besenbacher, and T. R. Jensen, "Complex hydrides for hydrogen storage - new perspectives," Mater. Today **17**, 122–128 (2014), https://doi.org/10.1016/j.mattod.2014.02.013.

[5] R. Mohtadi and S. Orimo, "The renaissance of hydrides as energy materials," Nat. Rev. Mater. **2**, 16091 (2016), https://doi.org/10.1038/natrevmats.2016.91.

[6] R. Yamagishi, T. Kojima, S. Kameoka, D. Okuyama, T. J. Sato, C. Nishimura, and A. P. Tsai, "Creating the hydrogen absorption capability of $CeNi_5$ through the addition of Al," Int. J. Hydrogen Energy **42**, 21832–21840 (2017), https://doi.org/10.1016/j.ijhydene.2017.07.072.

[7] M. Ihara, K. Tanaka, K. Sakaki, I. Honma, and K. Yamada, "Enhancement of the absorption coefficient of *cis*-$(NCS)_2$ Bis(2,2'-bipyridyl-4,4'-dicarboxylate)ruthenium(II) dye in dye-sensitized solar cells by a silver island film," J. Phys. Chem. B **101**, 5153–5157 (1997), https://doi.org/10.1021/jp963931z.

[8] D. Pacifici, H. J. Lezec, and H. A. Atwater, "All-optical modulation by plasmonic excitation of CdSe quantum dots," Nat. Photon. **1**, 402–406 (2007), https://doi.org/10.1038/nphoton.2007.95.

[9] J. A. Schuller, E. S. Barnard, W. S. Cai, Y. C. Jun, J. S. White, and M. L. Brongersma, "Plasmonics for extreme light concentration and manipulation," Nat. Mater. **9**, 193–204 (2010), https://doi.org/10.1038/NMAT2630.

[10] A. I. Kuznetsov, A. E. Miroshnichenko, M. L. Brongersma, Y. S. Kivshar, and B. Luk'yanchuk, "Optically resonant dielectric nanostructures," Science **354**, aag2472 (2016), https://doi.org/10.1126/science.aag2472.

[11] A. Kristensen, J. K. W. Yang, S. I. Bozhevolnyi, S. Link, P. Nordlander, N. J. Halas, and N. A. Mortensen, "Plasmonic colour generation," Nat. Rev. Mater. **2**, 16088 (2017), https://doi.org/10.1038/natrevmats.2016.88.

[12] V. G. Kravets, A. V. Kabashin, W. L. Barnes, and A. N. Grigorenko, "Plasmonic surface lattice resonances: A review of properties and applications," Chem. Rev. **118**, 5912–5951 (2018), https://doi.org/10.1021/acs.chemrev.8b00243.

[13] C. Langhammer, I. Zoric, B. Kasemo, and B. M. Clemens, "Hydrogen storage in Pd nanodisks characterized with a novel nanoplasmonic sensing scheme," Nano Lett. **7**, 3122–3127 (2007), https://doi.org/10.1021/nl071664a.

[14] N. Liu, M. L. Tang, M. Hentschel, H. Giessen, and A. P. Alivisatos, "Nanoantenna-enhanced gas sensing in a single tailored nanofocus," Nat. Mater. **10**, 631–636 (2011), https://doi.org/10.1038/NMAT3029.

[15] A. Baldi, T. C. Narayan, A. L. Koh, and J. A. Dionne, "*In situ* detection of hydrogen-induced phase transitions in individual palladium nanocrystals," Nat. Nater. **13**, 1143–1148 (2014), https://doi.org/10.1038/NMAT4086.

[16] F. A. A. Nugroho, I. Darmadi, L. Cusinato, A. Susarrey-Arce, H. Schreuders, L. J. Bannenberg, A. B. da Silva Fanta, S. Kadkhodazadeh, J. B. Wagner, T. J. Antosiewicz, A. Hellman, V. P. Zhdanov, B. Dam, and C. Langhammer, "Metal–polymer hybrid nanomaterials

for plasmonic ultrafast hydrogen detection," Nat. Mater. **18**, 489–495 (2019), https://doi.org/10.1038/s41563-019-0325-4.

[17] R. Kodama, P. A. Norreys, K. Mima, A. E. Dangor, R. G. Evans, H. Fujita, Y. Kitagawa, K. Krushelnick, T. Miyakoshi, N. Miyanaga, T. Norimatsu, S. J. Rose, T. Shozaki, K. Shigemori, A. Sunahara, M. Tampo, K. A. Tanaka, Y. Toyama, T. Yamanaka, and M. Zepf, "Fast heating of ultrahigh-density plasma as a step towards laser fusion ignition," Nature **412**, 798–802 (2001), https://doi.org/10.1038/35090525.

[18] Y. Iwamura, M. Sakano, and T. Itoh, "Elemental analysis of Pd complexes: Effects of D_2 gas permeation," Jpn. J. Appl. Phys. **41**, 4642–4650 (2002), https://doi.org/10.1143/JJAP.41.4642.

[19] L. Holmlid and S. Olafsson, "Charged particle energy spectra from laser-induced processes: Nuclear fusion in ultra-dense deuterium D(0)," Int. J. Hydrogen Energy **41**, 1080–1088 (2016), https://doi.org/10.1016/j.ijhydene.2015.10.072.

[20] F. M. Prados-Estévez, A. V. Subashiev, and H. H. Nee, "Strong screening by lattice confinement and resultant fusion reaction rates in fcc metals," Nucl. Instrum. Methods Phys. Res. B **407**, 67–72 (2017), https://doi.org/10.1016/j.nimb.2017.05.047.

[21] S. La Pape, L. F. Berzak Hopkins, L. Divol, A. Pak, E. L. Dewald, S. Bhandarkar, L. R. Bennedetti, T. Bunn, J. Biener, J. Crippen, D. Casey, D. Edgell, D. N. Fittinghoff, M. Gatu-

Johnson, C. Goyon, S. Haan, R. Hatarik, M. Havre, D. D. Ho, N. Izumi, J. Jaquez, S. F. Khan, G. A. Kyrala, T. Ma, A. J. Mackinnon, A. G. MacPhee, B. J. MacGowan, N. B. Meezan, J. Milovich, M. Millot, P. Michel, S. R. Nagel, A. Nikroo, P. Patel, J. Ralph, J. S. Ross, N. G. Rice, D. Strozzi, M. Stadermann, P. Volegov, C. Yeamans, C. Weber, C. Wild, D. Callahan, and O. A. Hurricane, "Fusion energy output greater than the kinetic energy of an imploding shell at the National Ignition Facility," Phys. Rev. Lett. **120**, 245003 (2018), https://doi.org/10.1103/PhysRevLett.120.245003.

[22] N. Fukuoka and K. Tanabe, "Large plasmonic field enhancement on hydrogen-absorbing transition metals at lower frequencies: Implications for hydrogen storage, sensing, and nuclear fusion," J. Appl. Phys. **126**, 023102 (2019), https://doi.org/10.1063/1.5091723.

[23] K. Tanabe, "Field enhancement around metal nanoparticles and nanoshells: A systematic investigation," J. Phys. Chem. C **112**, 15721–15728 (2008), https://doi.org/10.1021/jp8060009.

[24] N. Fukuoka and K. Tanabe, "Lightning-rod effect of plasmonic field enhancement on hydrogen-absorbing transition metals," Nanomaterials **9**, 1235 (2019), https://doi.org/10.3390/nano9091235.

[25] P. K. Aravind, A. Nitzan, and H. Metiu, "The interaction between electromagnetic resonances and its role in spectroscopic studies of molecules adsorbed on colloidal particles or metal spheres," Surf. Sci. **110**, 189–204 (1981), https://doi.org/10.1016/0039-6028(81)90595-1.

[26] M. Inoue and K. Ohtaka, "Surface enhanced Raman scattering by metal spheres. I. Cluster effect," J. Phys. Soc. Jpn. **52**, 3853–3864 (1983), https://doi.org/10.1143/JPSJ.52.3853.

[27] J. A. Dionne, L. A. Sweatlock, H. A. Atwater, and A. Polman, "Plasmon slot waveguides: Towards chip-scale propagation with subwavelength-scale localization," Phys. Rev. B **73**, 035407 (2006), https://doi.org/10.1103/PhysRevB.73.035407.

[28] W. Kubo and S. Fujikawa, "Au double nanopillars with nanogap for plasmonic sensor," Nano Lett. **11**, 8–15 (2011), https://doi.org/10.1021/nl100787b.

[29] W. Zhou, M. Dridi, J. Y. Suh, C. H. Kim, D. T. Co, M. R. Wasielewski, G. C. Schatz, and T. W. Odom, "Lasing action in strongly coupled plasmonic nanocavity arrays," Nat. Nanotechnol. **8**, 506–511 (2013), https://doi.org/10.1038/NNANO.2013.99.

[30] M. Ludwig, G. Aguirregabiria, F. Ritzkowsky, T. Rybka, D. C. Marinica, J. Aizpurua, A. G. Borisov, A. Leitenstorfer, and D. Brida, "Sub-femtosecond electron transport in a nanoscale gap," Nat. Phys. **16**, 341–345 (2020), https://doi.org/10.1038/s41567-019-0745-8.

[31] P. M. Morse and H. Feshbach, Methods of Theoretical Physics, McGraw-Hill, New York (1953).

[32] J. D. Jackson, Classical Electrodynamics, Wiley, New York (1975).

[33] E. D. Palik, Handbook of Optical Constants of Solids, Academic Press, Orlando (1985).

[34] F. Di Pascasio, D. Gozzi, B. Panella, and C. Trionfetti, "H_2 plasma for hydrogen loading in Pd," Intermetallics **11**, 1345–1354 (2003), https://doi.org/10.1016/S0966-9795(03)00178-X.

[35] E. A. Hodille, N. Fernandez, Z. A. Piazza, M. Ajmalghan, and Y. Ferro, "Hydrogen supersaturated layers in H/D plasma-loaded tungsten: A global model based on thermodynamics, kinetics and density functional theory data," Phys. Rev. Mater. **2**, 093802 (2018), https://doi.org/10.1103/PhysRevMaterials.2.093802.

[36] S. J. Oldenburg, R. D. Averitt, S. L. Westcott, and N. J. Halas, "Nanoengineering of optical resonances," Chem. Phys. Lett. **288**, 243–247 (1998), https://doi.org/10.1016/S0009-2614(98)00277-2.

[37] M. B. Mohamed, V. Volkov, S. Link, M. A. El-Sayed, "The 'lightning' gold nanorods: Fluorescence enhancement of over a million compared to the gold metal," Chem. Phys. Lett. **317**, 517–523 (2000), https://doi.org/10.1016/S0009-2614(99)01414-1.

FIGURE CAPTIONS

FIG. 1. Schematic configuration of the bipartite system for the calculations of field enhancement factors.

FIG. 2. Calculated spectra of electromagnetic field enhancement factor for Pd particles in air, H_2, or vacuum, for the condition θ_0 = (a) 0, (b) π/2, (c) π/4, θ = π, and D/R_0 = 0.1, with various d/D.

FIG. 3. Calculated electromagnetic field enhancement factors for Pd particles in air, H_2, or vacuum, for the condition θ_0 = 0, d/D = 0, and λ = 365 nm, with various θ and D/R_0.

FIG. 4. Calculated spectra of electromagnetic field enhancement factor for Pd particles in air, H_2, or vacuum, for the condition θ_0 = 0, θ = π, and d/D = (a) 0, (b) 0.5, with various D/R_0.

FIG. 5. Calculated spectra of electromagnetic field enhancement factor for various metal particles in air, H_2, or vacuum, for the condition θ_0 = 0, θ = π, D/R_0 = (a, b) 0.1, (c, d) 0.01, and d/D = (a, c) 0, (b, d) 0.5.

FIG. 6. Calculated spectra of electromagnetic field enhancement factor for various metal particles in H_2O, for the condition $\theta_0 = 0$, $\theta = \pi$, D/R_0 = (a, b) 0.1, (c, d) 0.01, and d/D = (a, c) 0, (b, d) 0.5.

FIGURES

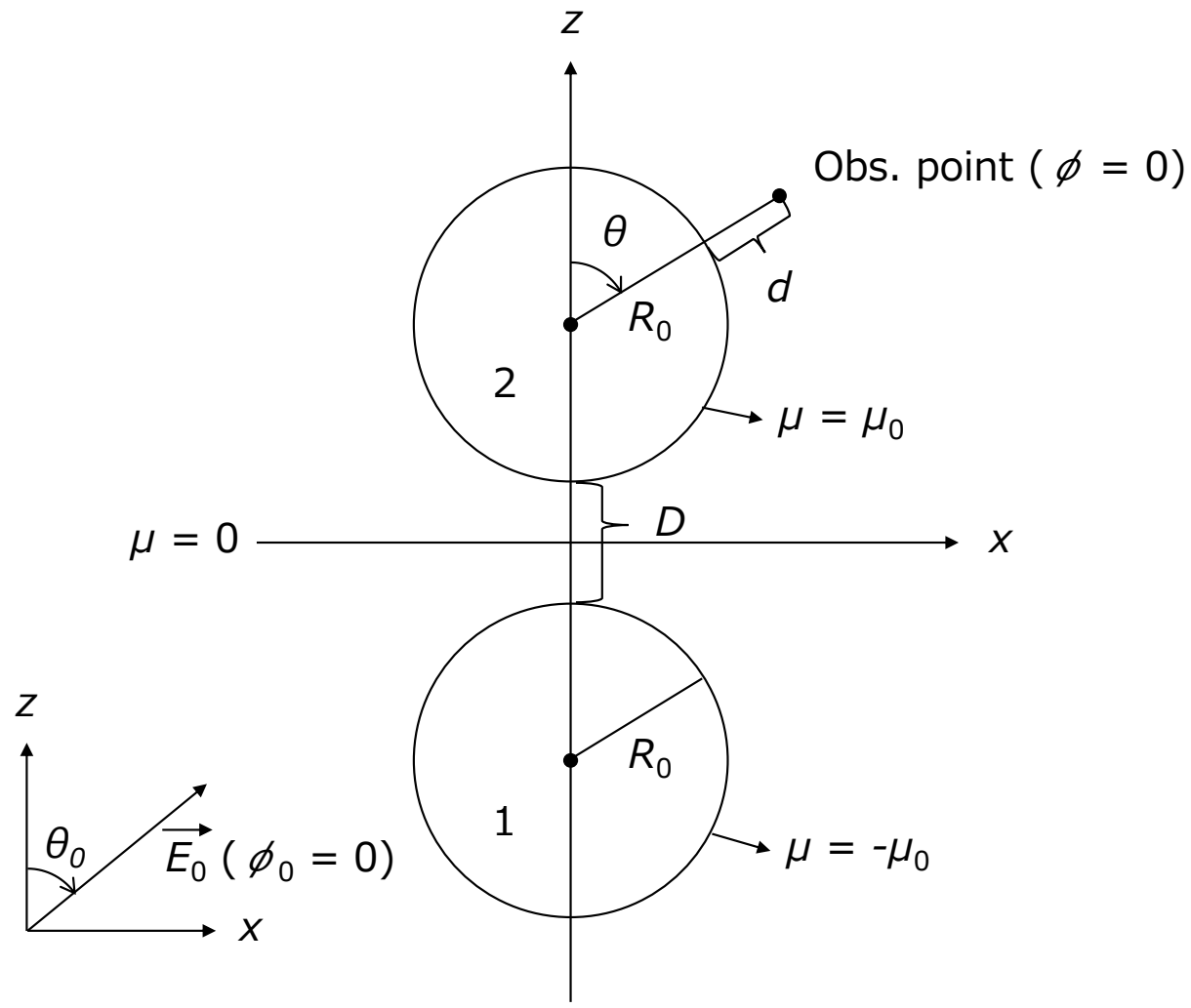

FIG. 1.

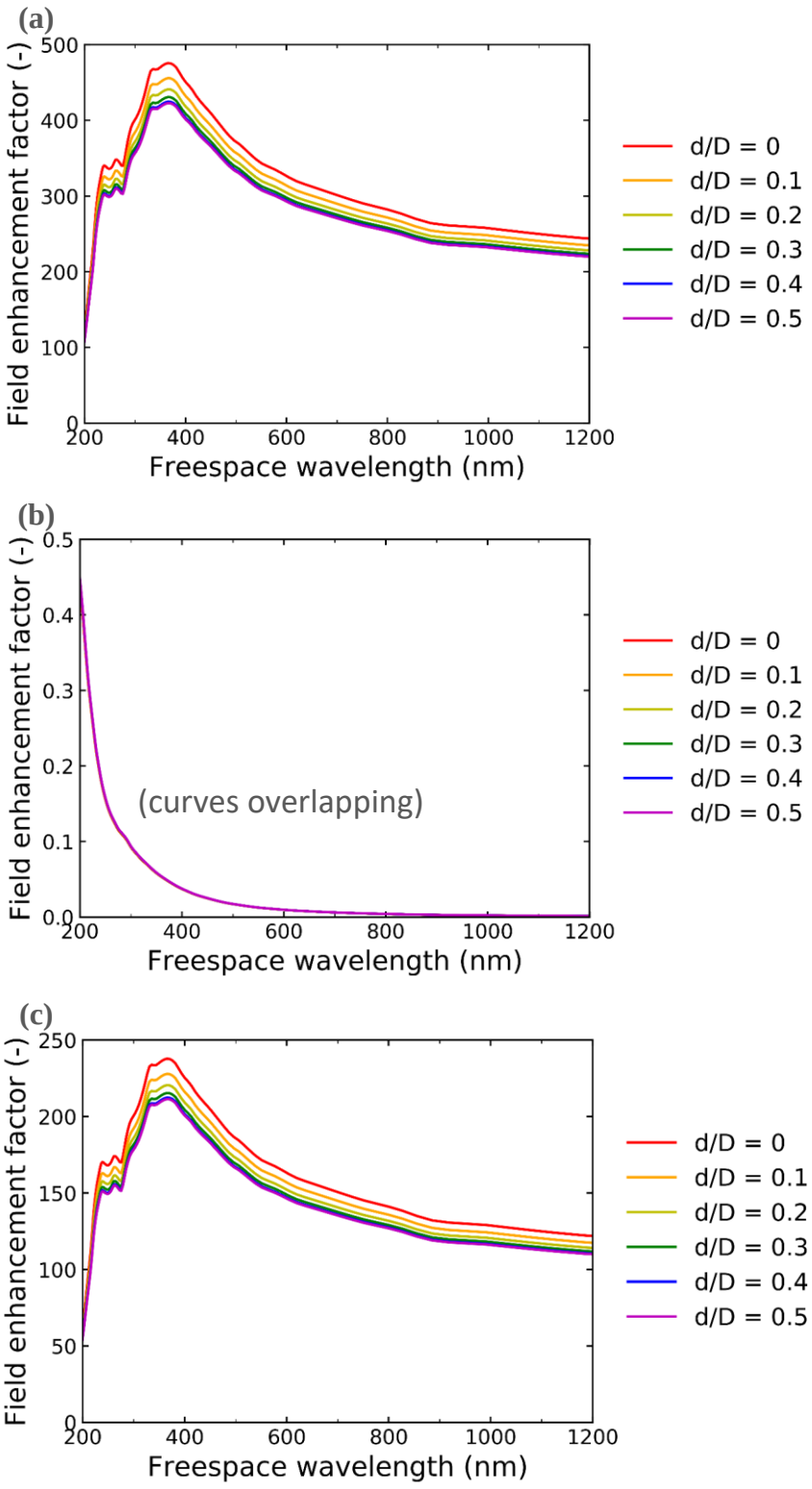
(a)
Field enhancement factor (-)
Freespace wavelength (nm)
d/D = 0
d/D = 0.1
d/D = 0.2
d/D = 0.3
d/D = 0.4
d/D = 0.5
(b)
Field enhancement factor (-)
(curves overlapping)
Freespace wavelength (nm)
d/D = 0
d/D = 0.1
d/D = 0.2
d/D = 0.3
d/D = 0.4
d/D = 0.5
(c)
Field enhancement factor (-)
Freespace wavelength (nm)
d/D = 0
d/D = 0.1
d/D = 0.2
d/D = 0.3
d/D = 0.4
d/D = 0.5

FIG. 2.

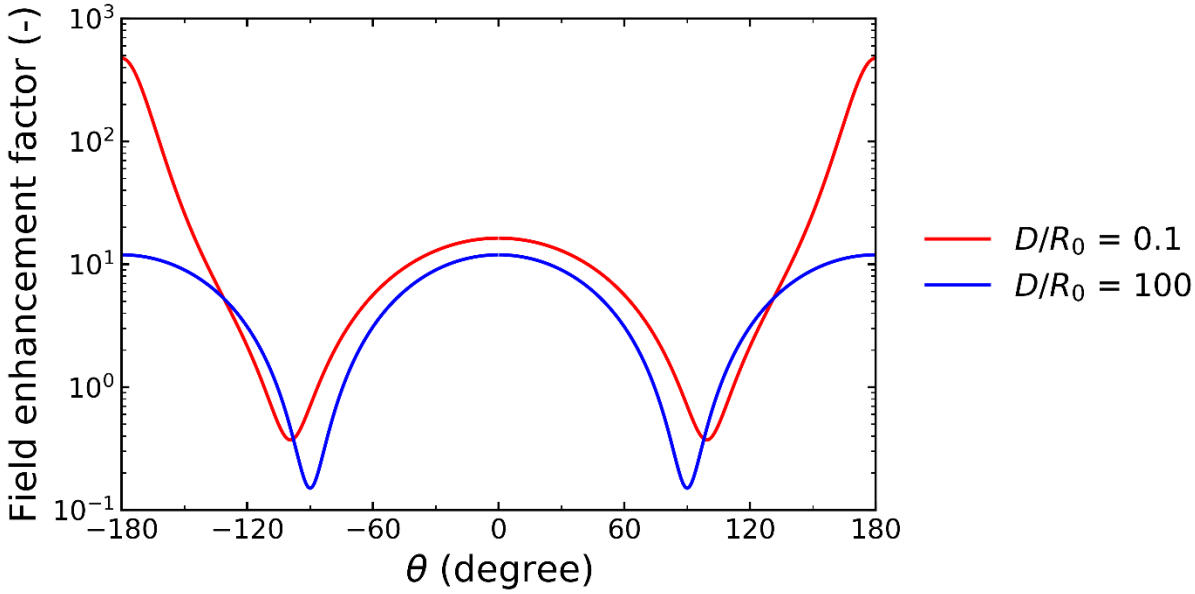
Field enhancement factor (-)
10^3
10^2
10^1
10^0
10^{-1}
−180
−120
−60
0
60
120
180
θ (degree)
D/R_0 = 0.1
D/R_0 = 100

FIG. 3.

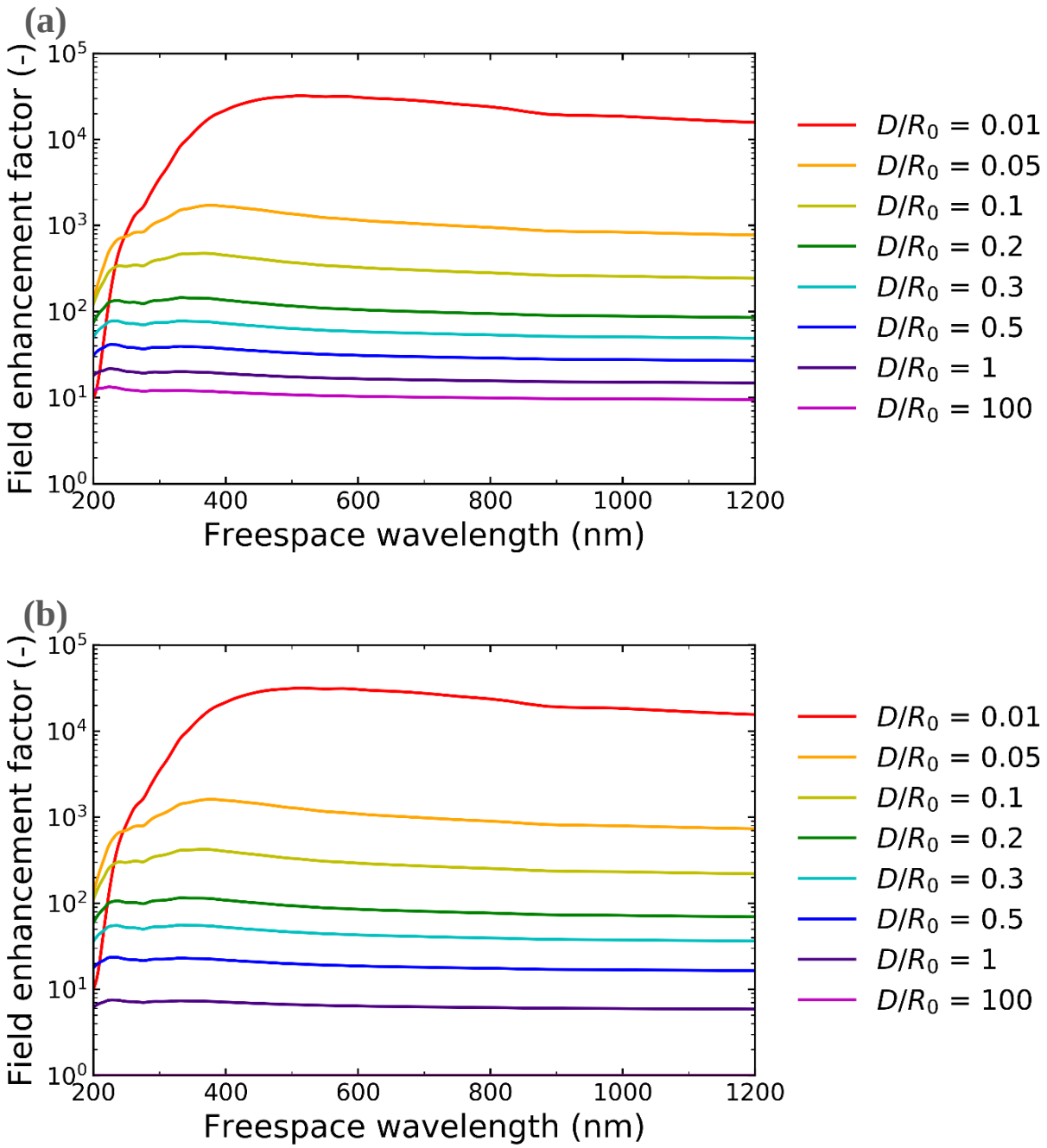
(a)
Field enhancement factor (-)
Freespace wavelength (nm)
D/R_0 = 0.01
D/R_0 = 0.05
D/R_0 = 0.1
D/R_0 = 0.2
D/R_0 = 0.3
D/R_0 = 0.5
D/R_0 = 1
D/R_0 = 100
(b)
Field enhancement factor (-)
Freespace wavelength (nm)
D/R_0 = 0.01
D/R_0 = 0.05
D/R_0 = 0.1
D/R_0 = 0.2
D/R_0 = 0.3
D/R_0 = 0.5
D/R_0 = 1
D/R_0 = 100

FIG. 4.

(a), shorter wavelength

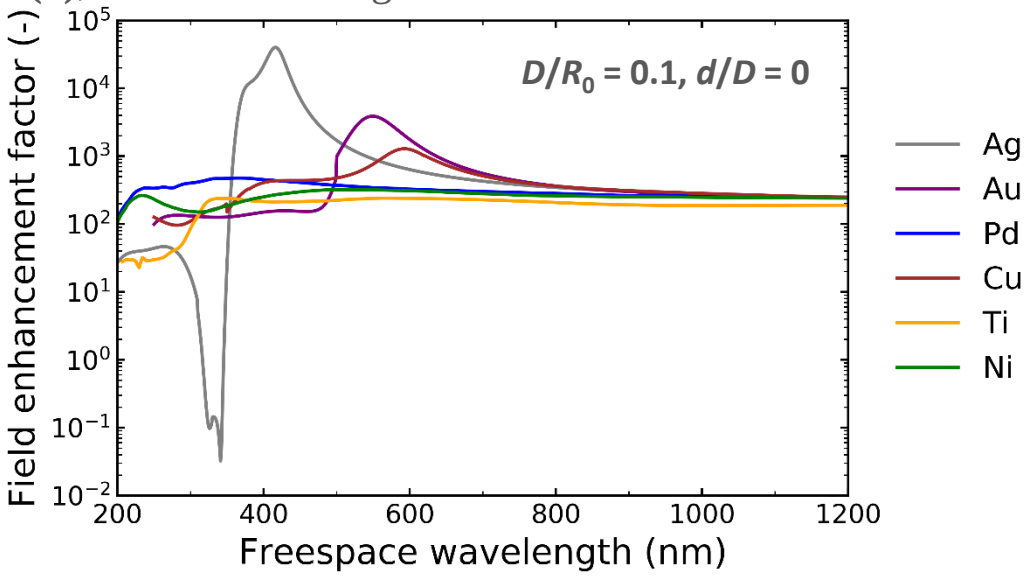

(a), longer wavelength

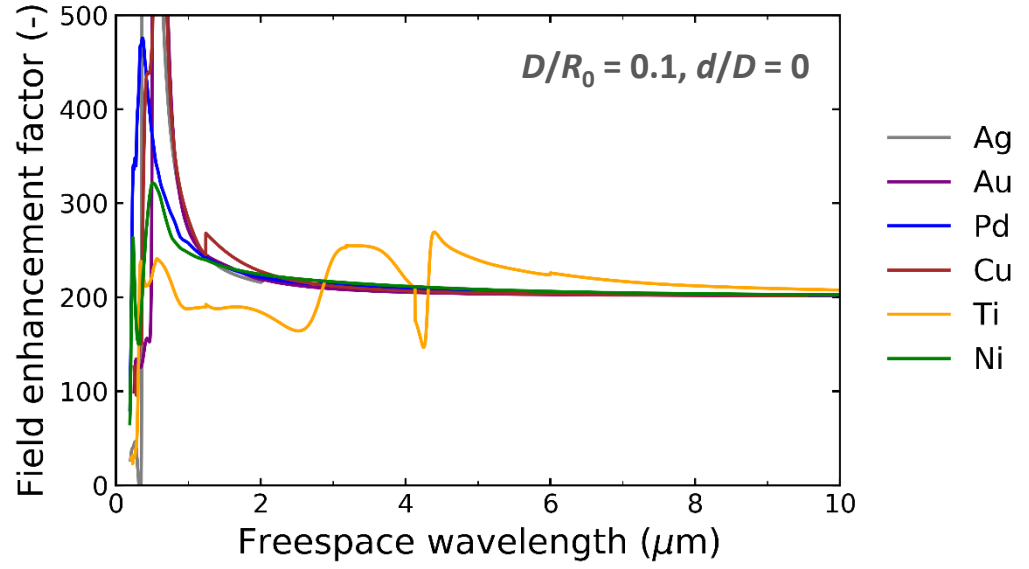

FIG. 5 (a).

(b), shorter wavelength

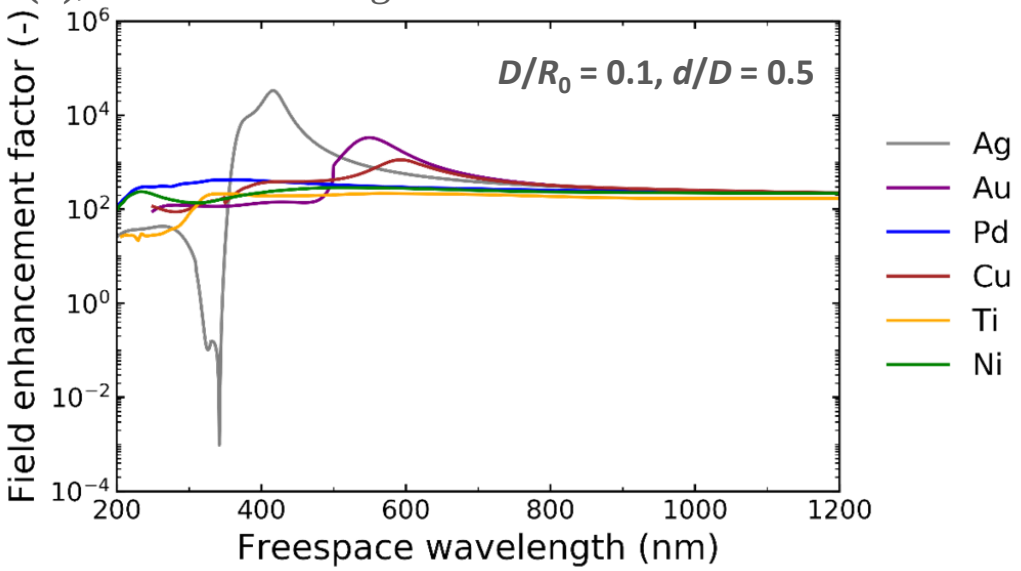

(b), longer wavelength

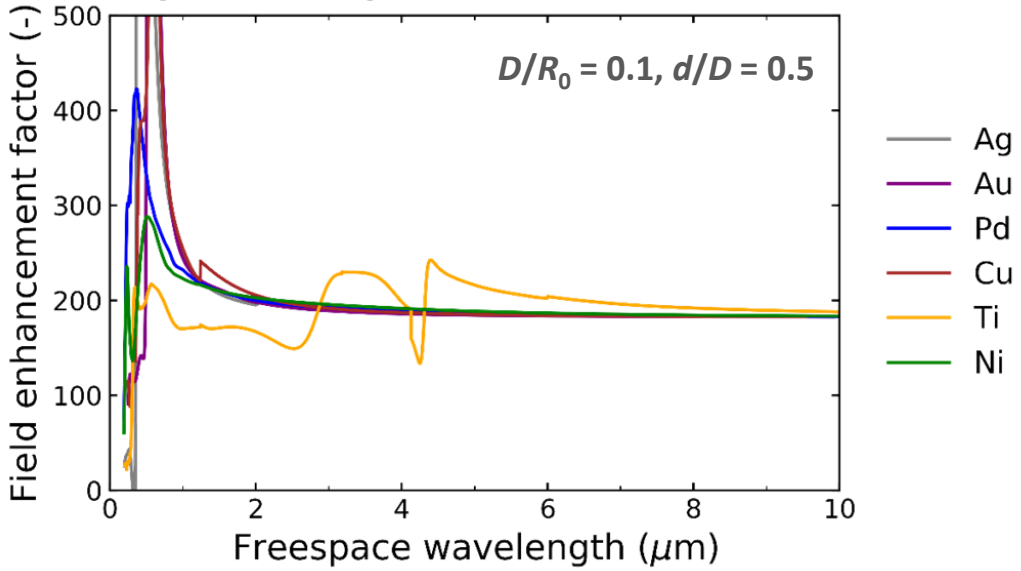

FIG. 5 (b).

(c), shorter wavelength

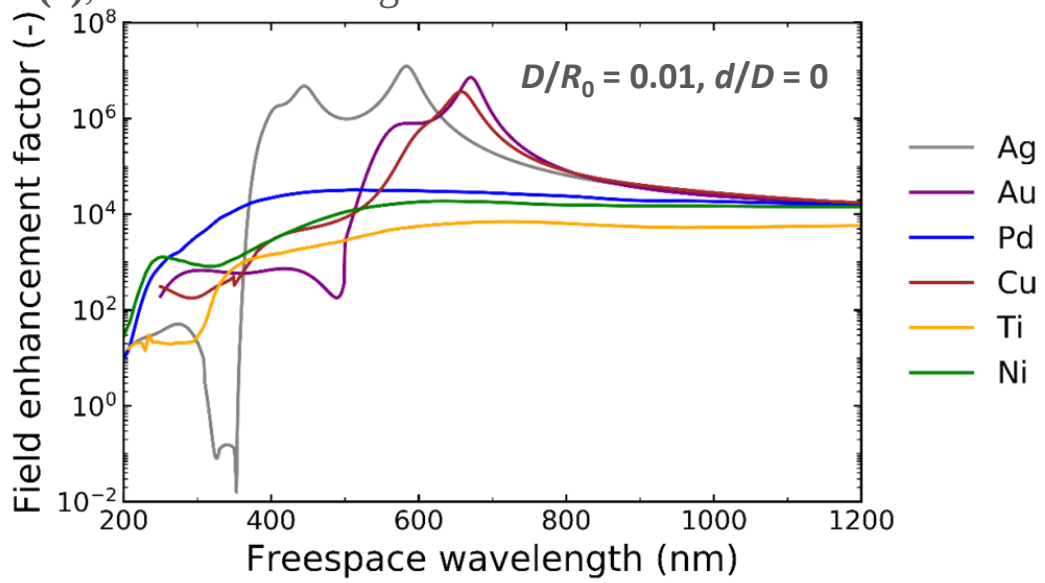

(c), longer wavelength

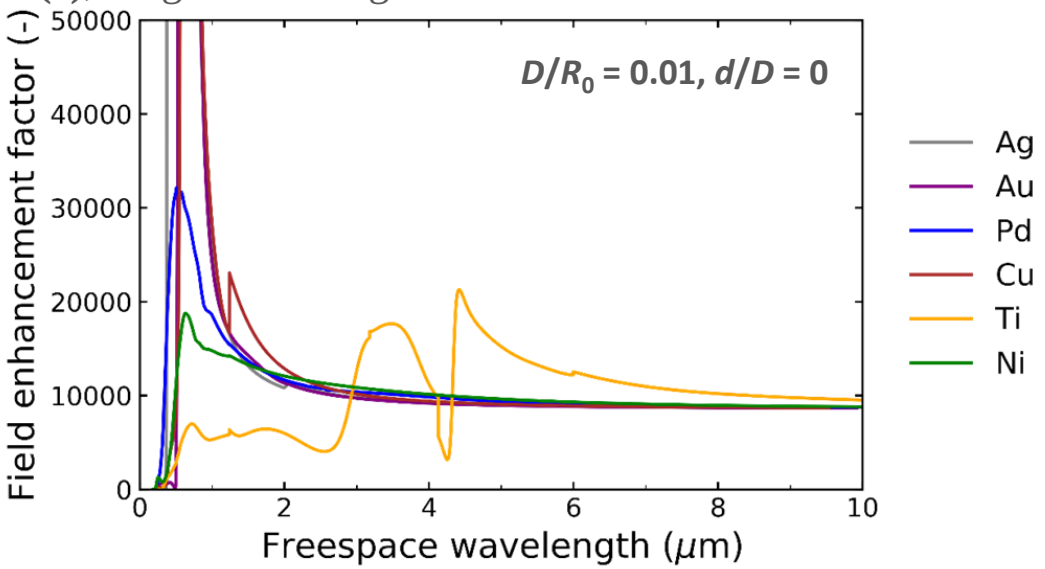

FIG. 5 (c).

(d), shorter wavelength

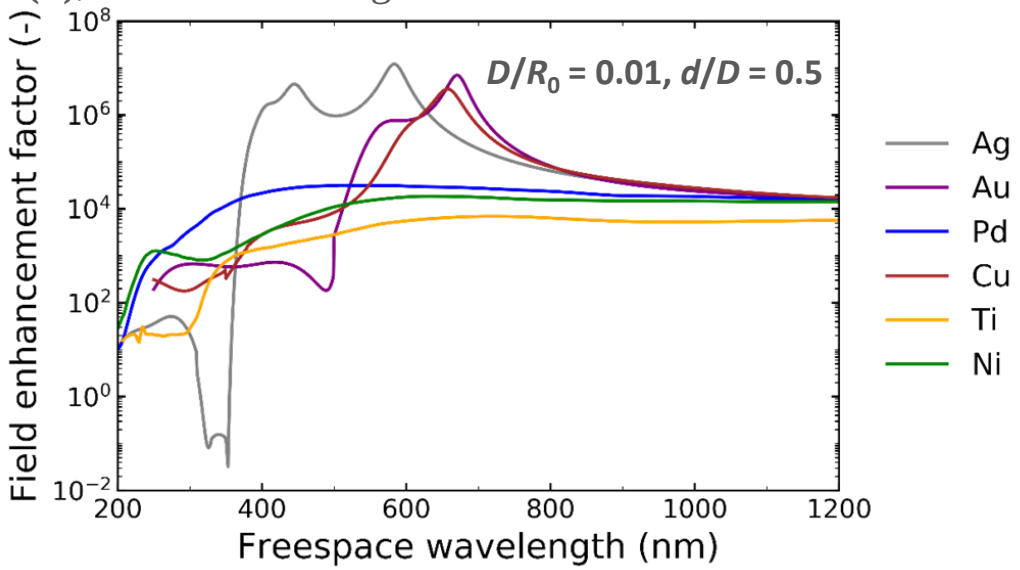

(d), longer wavelength

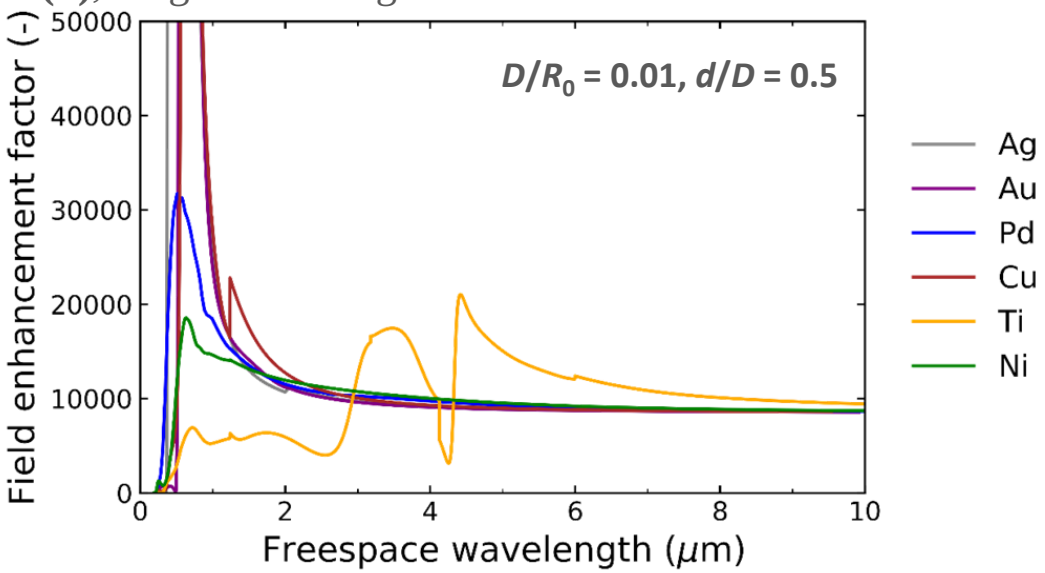

FIG. 5 (d).

(a), shorter wavelength

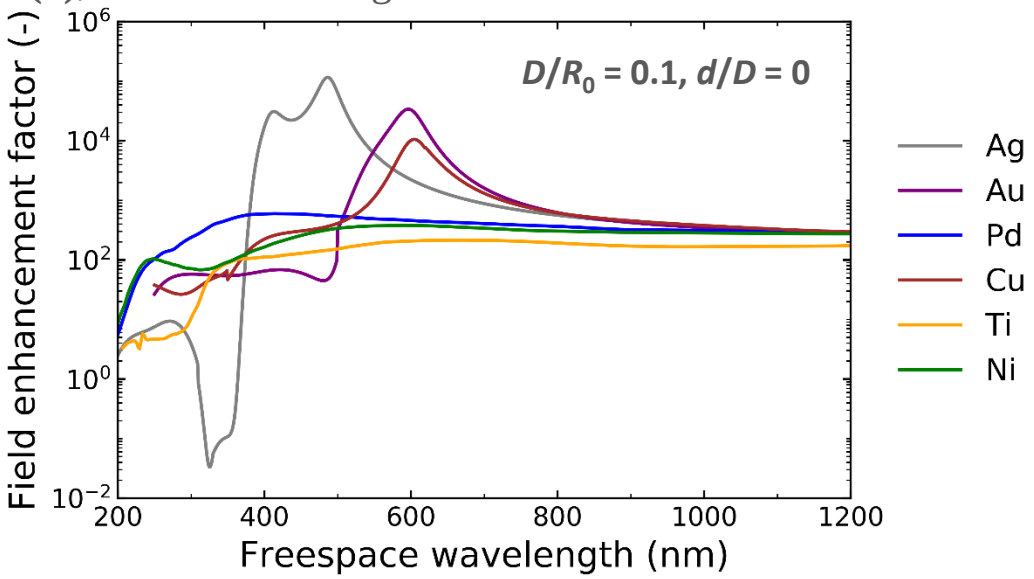

(a), longer wavelength

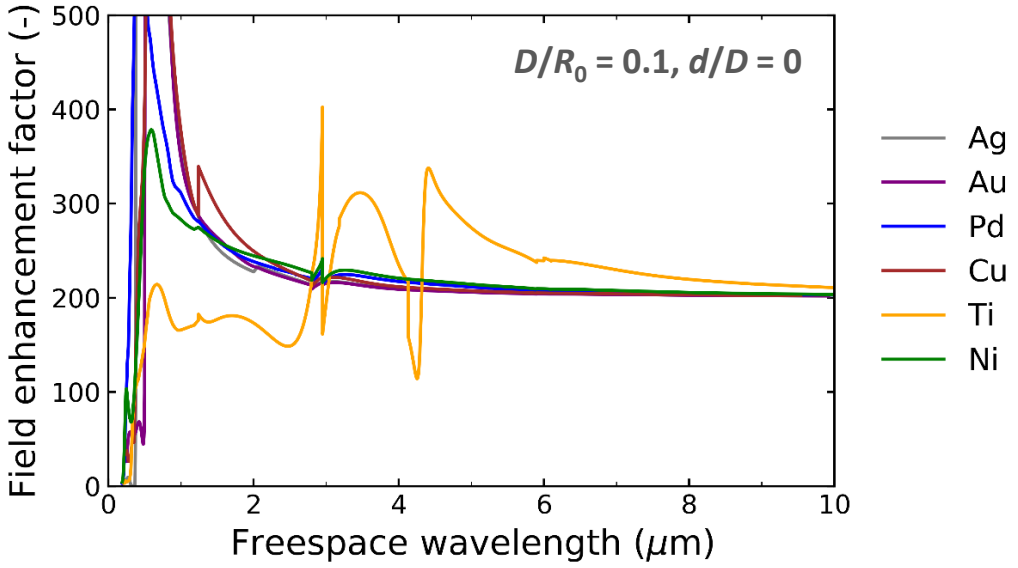

FIG. 6 (a).

(b), shorter wavelength

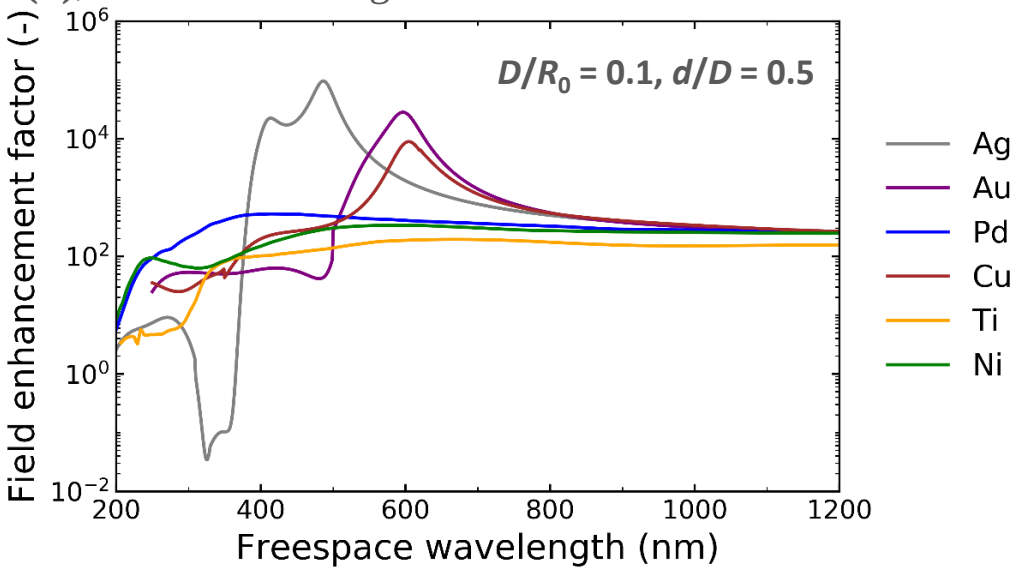

(b), longer wavelength

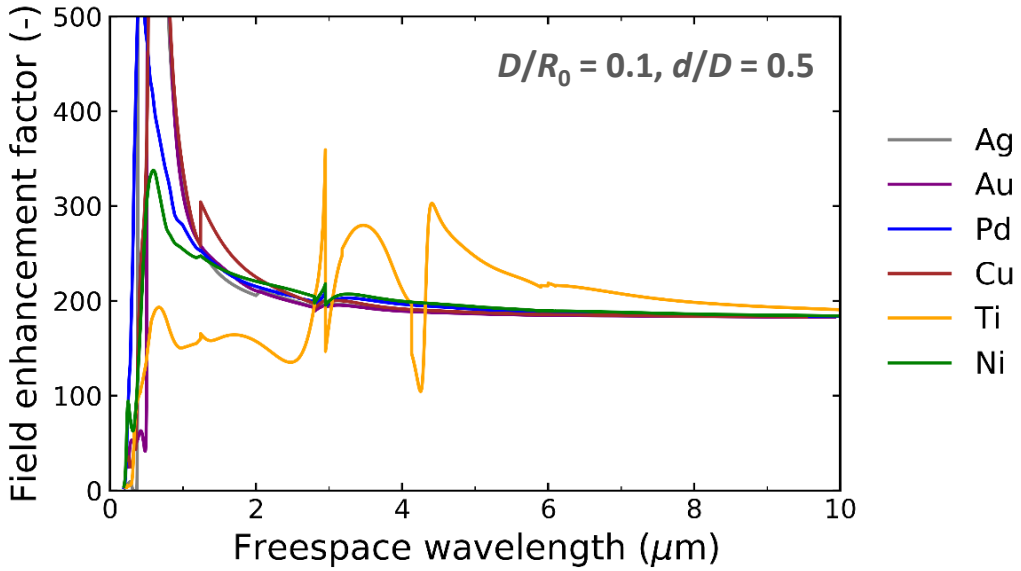

FIG. 6 (b).

(c), shorter wavelength

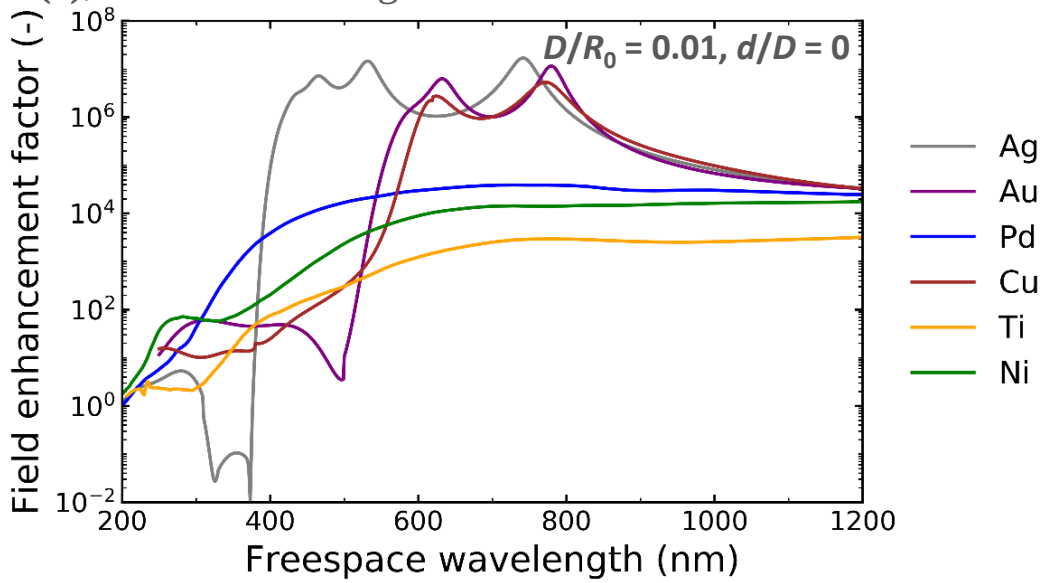

(c), longer wavelength

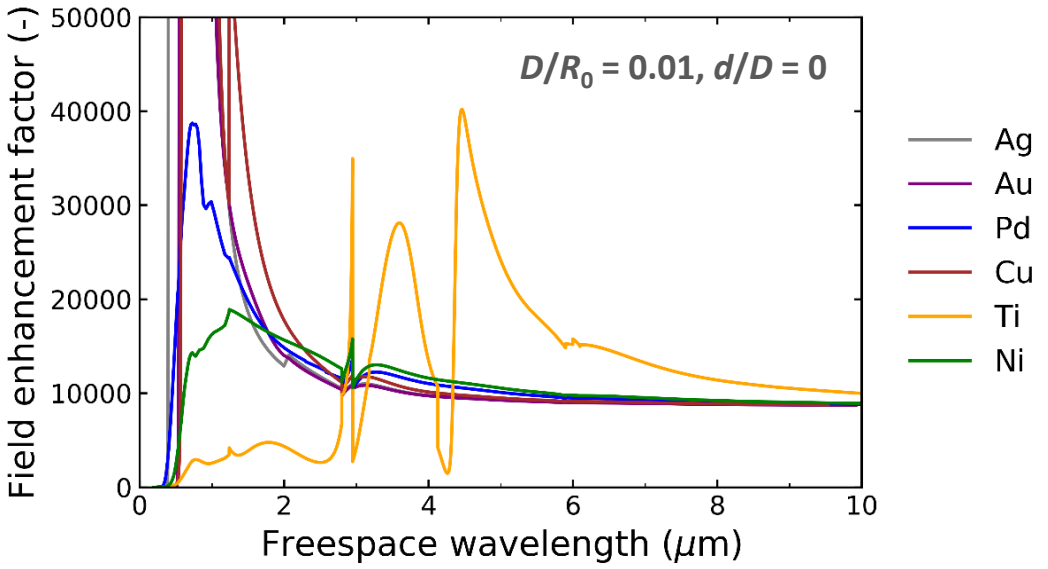

FIG. 6 (c).

(d), shorter wavelength

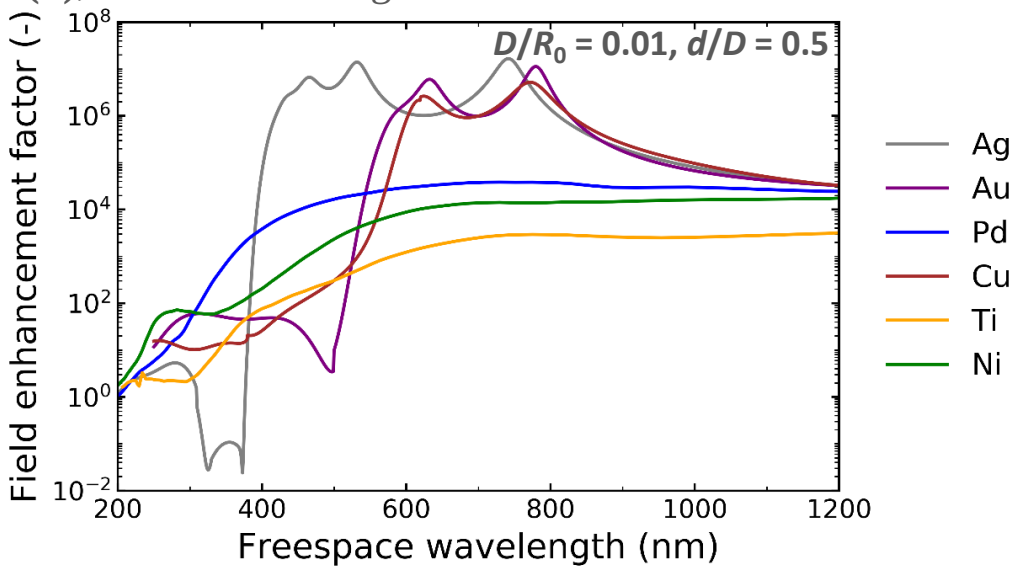

(d), longer wavelength

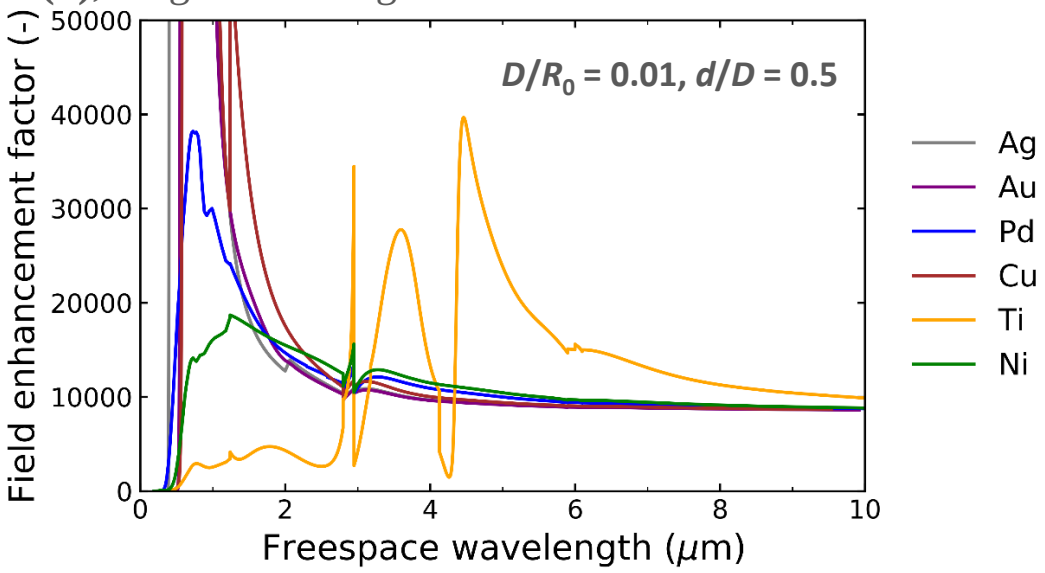

FIG. 6 (d).